Geoscience Laser Altimeter System (GLAS)

Algorithm Theoretical Basis Document
Version 2.0

TIDAL CORRECTIONS

Prepared by:

Helen A. Phillips, Jeff R. Ridgway, Jean-Bernard Minster
Institute of Geophysics and Planetary Physics
Scripps Institution of Oceanography
La Jolla CA 92093-0225

Donghui Yi
Raytheon ITSS
Oceans and Ice Branch, Code 971
NASA Goddard Space Flight Center
Greenbelt MD 20771

Charles Bentley
Geophysical and Polar Research Center
University of Wisconsin
Madison, WI

August 1999

1. Introduction

This Algorithm Theoretical Basis Document deals with the tidal corrections that need to be applied to range measurements made by the Geoscience Laser Altimeter System (GLAS). These corrections result from the action of ocean tides and Earth tides which lead to deviations from an equilibrium surface. Since the effect of tides is dependent of the time of measurement, it is necessary to remove the instantaneous tide components when processing altimeter data, so that all measurements are made to the equilibrium surface.

The three main tide components to consider are the ocean tide, the solid-earth tide and the ocean loading tide. There are also long period ocean tides and the pole tide. The approximate magnitudes of these components are illustrated in Table 1, together with estimates of their uncertainties (i.e. the residual error after correction). All of these components are important for GLAS measurements over the ice sheets since centimeter-level accuracy for surface elevation change detection is required. The effect of each tidal component is to be removed by approximating their magnitude using tidal prediction models. Conversely, assimilation of GLAS measurements into tidal models will help to improve them, especially at high latitudes.

2. Background

The Antarctic and Greenland ice sheets contain enough water to produce a 72-m rise in sea-level if they were to melt (*Oerlemans*, 1993). For this reason alone, we need to understand how Antarctica and Greenland will respond to climate change. During the present century, sea-level has risen at an average rate of 1.0-2.0 mm yr^{-1} (*Warrick*, 1993). Part of the sea level rise can be explained by ocean thermal expansion and the melting of glaciers and small ice caps and, perhaps, net mass loss to the Greenland ice sheet. The amount of snow that falls each year on the grounded Antarctic ice is equivalent to about 5 mm yr^{-1} of global sea level change (*Jacobs*, 1992), so annual variation of snow accumulation on the Antarctic ice sheet can have a measurable effect on sea level. Without independent knowledge of the contribution of the Antarctic ice sheet, there remains a major uncertainty in understanding sea level change (*Warrick and Oerlemans*, 1990). To fix ideas, assuming that half of the sea-level rise, i.e. 0.5-1.0 mm yr^{-1}, comes from a mass loss to the Antarctic ice sheet, then the mean elevation of Antarctica would need to drop at a rate of about 15-30 mm yr^{-1}. This estimate ignores the potential contributions of other phenomena, such as post-glacial rebound.

Satellite altimeters can be used to monitor the volume of the polar ice sheets. Substantial progress in studying polar mass balance has been sustained by the use of satellite radar altimeters (*Brenner et al*, 1983, *Zwally et al*, 1989, *Zwally*, 1989, *Partington et al*, 1991, *Bentley and Sheehan*, 1992, *Lingle et al*, 1994, *Yi et al*, 1997). However the precision of the satellite radar altimeters is limited by surface slope because of the large radar footprint (*Brenner et al*, 1983), imperfect understanding of the microwave penetration to the subsnow surface (*Ridley and Partington*, 1988, *Yi and Bentley*, 1997), and inadequate accuracy of satellite orbits (*Haines et al*, 1994). The Geoscience Laser Altimeter System (GLAS) (*Schutz*, 1995), designed primarily for measuring the surface elevation of the polar ice sheets, has a much smaller footprint of about 70 m which will reduce the surface slope effect and benefits from an on-board GPS which will give an orbit accuracy of ±50 mm.

Ocean tides and solid earth tides have been taken into account in processing the satellite

radar altimetry data (e.g. *Zwally et al*, 1990). However, the smaller vertical displacement caused by the ocean tidal loading has not previously been given much attention. This is because the precision of satellite radar altimeters over land is of the order of several tens of centimeters while the vertical displacement load tide is only of the order of several tens of millimeters even along the coast. Ocean loading effects only become important when the surface elevation measurements require centimeter-level precision. To determine surface elevation accurately and to detect surface elevation change, it is important to estimate the ocean tidal loading effects and apply an ocean tidal loading correction to the surface elevation measurement.

3. 'Standard' tide corrections

Several of the tide corrections listed in Table 1 will be removed from GLAS range measurements by applying 'standard' models that have been successfully used for previous satellite altimeter missions such as ERS-1, ERS-2 and TOPEX/Poseidon. These corrections are the solid earth tide, long-period tides and pole tide.

- **Solid earth tide** The solid earth tide is the periodic movement of the Earth's crust caused by gravitational interactions between the Sun, Moon and Earth. The magnitude of this tide is $\pm$30cm, and its effect should be removed for GLAS through modeling, in the same way as it was for TOPEX/Poseidon. This was done using TOPEX/Poseidon document "g1062" (with the tested algorithm 'TIDPOT.FOR')

- **Long-period tides** Equilibrium long period tides are removed by models which are based on the Cartwright-Taylor-Edden tide potential. Any reliable code (such as subroutine 'lpeqmt', written by *Cartwright* (1990)) that is used for TOPEX/Poseidon should be used for its calculation for the GLAS records, independently of the diurnal/semidiurnal ocean tide model used. The non-equilibrium long-period tide should probably be ignored, as it is small and no model for it has yet been finalized.

- **Pole tide** This tide results from polar motion has component periods mainly of 12 months and 14 months. It should be calculated for GLAS after TOPEX/Poseidon algorithm document g1063.

4. Ocean tide correction

4.1 Ocean regions

Tides over the open ocean will be removed from GLAS range measurements by applying a ocean tide model. This tide model should ideally be global, include predictions for the Arctic and the Antarctic, and be familiar to the TOPEX/Poseidon software team. Two suitable models are CSR3.0 (*Eanes*, 1994; used for TOPEX/Poseidon) and FES95.2 (*Le Provost et al.*, 1998), and these two models compare fairly well in the open ocean *(Shum et al.,* 1997*)*. Although CSR3.0 was used for TOPEX/Poseidon, it is not reliable below 78°S. We therefore recommend that the FES95.2 model is adopted as the primary global model for GLAS ocean tide corrections. This is an improvement of the FES94.1 model as it assimilates into the hydrodynamic model the earlier empirical TOPEX/Poseidon CSR2.0 tidal solution using the representer methods developed by

Egbert et al. (1994). The CSR2.0 solutions were derived in 1994 at the University of Texas, from a two year time series of TOPEX/Poseidon data. The standard release of the FES95.2 solutions is 0.5° x 0.5° for ocean depths greater than 1000 m. The tidal correction at a specific location and time will be interpolated based on their location within this grid.

We also recommend that a second model be considered for application around Antarctica. This is the Circum-Antarctic Tidal Simulation model (CATS99.2), developed at the Earth and Space Science Center, Seattle, Washington by Laurence Padman (*Rignot et al.* 1999). The CATS99.2 model covers the entire globe south of 50°S, at a resolution of 0.25° in latitude (approximately 10 km around the Antarctic coast) and has been validated in the Weddell Sea region (*Robertson et al.* 1998) and at the front of the Filchner Ice Shelf (*Rignot et al.* 1999). The model comprises eight tidal constituents, five semidiurnal (M_2, S_2, K_2, N_2, and $2N_2$) and three diurnal (O_1, K_1, and Q_1). Incorporation of this model has the advantage that it is continuous at the boundary with the FES95.2 and would simply require a latitude switch so that this model is utilized below 50°S. However, it is noted that the process of 'matching' models at 50°S should be the object of careful analysis.

4.2 Ice shelves and glacier tongues

The floating parts of the ice sheets (ice shelves and floating glacier tongues) are displaced vertically in response to ocean tides. To assess elevation change in these regions, the instantaneous tide component must be removed from the elevation measurement, such that all ice shelf elevations are referred to an equilibrium surface. Modeling the tidal displacement of the floating ice shelves in response to ocean tides is not straightforward. There is currently no one model that accurately described the complex response of the floating parts of the Antarctic ice sheet to ocean tides. The CATS99.2 model has been shown to perform well at the ice front of the Filchner Ice Shelf (*Rignot et al.* 1999), but still requires work in other areas. This model will be improved as more observations from ice shelf tides (e.g. from *in situ* GPS, GLAS) and information on sub-ice-shelf water column thickness become available *(Laurence Padman, personal communication, July 1999).*

The vertical displacement of the ice shelves can be measured using kinematic GPS (e.g. *Vaughan 1994, 1995*) and static GPS (e.g. *Phillips et al. 1998*). For the Amery Ice Shelf, *Phillips et al* (*1998*) showed that the amplitude of the vertical tidal displacement at six sites on the central part of the ice shelf is the same as that predicted by a tide model for nearby Beaver Lake, provided by the National Tidal Facility, The Flinders University of South Australia. Static GPS observations collected on the Amery Ice Shelf during 1998-1999 have been processed in 1-hour segments within the GAMIT software *(Richard Coleman, personal communication, 1999).* The results indicate that there is a phase lag between the Beaver Lake Tide Model and the tidal response of the Amery Ice Shelf, with the Amery Ice Shelf ahead by around 65 minutes at the northernmost site (near the ice front) and 45 minutes at the southernmost site (near the grounding zone). The distance between these sites is approximately 400 km. A three-years series of field campaigns is planned for 1999-2000, 2000-1 and 2001-2. It is intended to use GLAS data acquired during the 90-day verification and validation phase of ICESat to generate new models (or improve existing models) for the major floating ice shelves, and these results will be validated using *in situ* observations from the Amery Ice Shelf. In addition to the data collected on the Amery Ice Shelf, we also recommend that long time series of static GPS data are collected on other ice shelves (e.g. Ross Ice Shelf, Ronne Ice Shelf, Filchner Ice Shelf) for further validation of ice shelf tide models.

When available, these ‘local’ models can potentially be added into higher level GLAS data products by specifying a mask for each region. This remains a research issue.

4.3 Land/Ocean mask

The resolution requirement for the Land/Ocean mask is higher for GLAS than it was for TOPEX/Poseidon. Application of a tidal model for GLAS requires a Land/Ocean mask that has a horizontal resolution of about 1 km. We recommend that:

1) the worldwide Generic Mapping Tool (GMT) database of *Wessel and Smith* (1996) be adopted. The implementation of Agnew (1996; see Section 4), has a resolution of 1/64 degree (1.7 km), saves disk space and is compatible with his load-tide software and is also recommended.

2) the Land/Ocean mask not be hard-coded but be stored as a readable file, which will be updated with more accurate values as they become available (e.g. for the floating ice extent of the Antarctic ice shelves). Sufficient flexibility should be programmed into the code such that higher-resolution versions of the land/ocean mask can be used as they are developed. Another consideration is the ‘transition zone’ of the Antarctic ice shelves. This is the region between the ‘limit of flexure’ i.e. the boundary between fully grounded and freely floating ice and the hydrostatic grounding line (the ‘hinge line’) which can extend for several kilometers *(Vaughan 1994)*. In this region, the ice does not respond freely to the ocean tides. Vaughan *(1995)* successfully modeled this as elastic plate flexure with an elastic modulus of about 0.88 GPa. However, we do not think that this should be calculated for incorporation into the GLAS records. This is a future topic of research and will be much improved with additional static GPS observations, information from Interferometric Synthetic Aperture Radar (InSAR) (e.g. *Rignot* 1998) and when GLAS data start becoming available.

5. Ocean-loading tide

The mass of water concentrated by the ocean tidal bulge is sufficient to compress the Earth’s lithosphere. As this mass is redistributed, elastic rebound of the lithosphere changes, and this is the ocean-loading tide. The vertical displacement caused by ocean-loading is of the order of several tens of millimeters in polar regions (Table 1), although it is primarily restricted to the vicinity of the coastline. Application of the ocean tidal loading correction will improve the accuracy of satellite laser altimeter measured surface elevation over the ice sheets, especially in the coastal areas.

5.1 Computation of ocean tidal loading

Various methods have been used to compute tidal loading. *Baker* (1985) lists five of them: (1) the spherical harmonic expansion method; (2) the polygon method; (3) the template method; (4) the spherical disc method; and (5) the Green’s function method. In this ATBD, the tidal loading is computed by the Green’s function method (*Farrell*, 1972). *Agnew* (1996) produced a software package which makes it is easy to calculate tidal loading at a given point by using the Green’s function and an ocean tide model. In Agnew’s package, the ocean load tide L is given by

$$L(\theta', \lambda') = \int_0^{2\pi} \left(\int_0^{\pi} \rho H(\theta, \lambda) G_L(\Delta) S_L(\alpha) a^2 \sin(\theta) d\theta \right) d\lambda \qquad (1)$$

where Δ is the distance, α is the azimuth of the point with geographical coordinates (θ, λ) relative to the place of observation, which is at (θ', λ'); H is the tidal height at (θ, λ), ρ is ocean water density, and a is the radius of the earth. G_L is the mass loading Green's function and S_L is the combination of trigonometric functions needed to compute a vector or tensor load. The Green functions used are obtained from *Farrell* (1972). As stated in Section 3.1, the global tide model we propose to use for the open ocean is the FES95.2 model (*Le Provost et al* 1998), and we would like to leave scope to include the CATS99.2 model below 50°S. Both of these models are compatible with Agnew's (1996) code (Duncan Agnew, personal communication, July 1999). In fact, local high accuracy models for specific locations, such as shallow seas (e.g. North Sea, English Channel, etc), or areas such as the Amery ice shelf, can be accommodated as well.

5. 2 Algorithm Description

The displacement component at a location at a time *t* is given by (*McCarthy*, 1992)

$$\Delta c = \sum_j f_j A_j \cos(\omega_j t + \chi_j + \mu_j - \Phi_j) \qquad (2)$$

where f_j and μ_j depend on the longitude of the lunar node, A_j and Φ_j are the amplitude and phase for each displacement component, ω_j is the frequency of tide *j* and χ_j is the astronomical argument at t = 0. The three components of displacement (vertical, east-west, north-south) can be calculated by the above equation, but here we are only interested in the vertical displacement. χ_j is calculated using the program ARG described by *McCarthy* (1992). f_j and μ_j are calculated by the following relations for the eight largest constituents, which together account for over 90% of the tidal signal (*Doodson*, 1928):

f_{m2} = 1.000 - 0.037 cos(N)

f_{s2} = 1.0

f_{n2} = 1.000 - 0.037 cos(N)

f_{k2} = 1.024 + 0.286 cos(N) + 0.008 cos(2N)

f_{k1} = 1.006 + 0.115 cos(N) - 0.009 cos(2N)

f_{o1} = 1.009 + 0.187 cos(N) - 0.015 cos(2N)

f_{p1} = 1.0

f_{q1} = 1.009 + 0.187 cos(N) - 0.015 cos(2N)

μ_{m2} = -2.1° sin(N)

μ_{s2} = 0.0°

μ_{n2} = -2.1° sin(N)

μ_{k2} = -17.7° sin(N) + 0.7° sin(2N)

μ_{k1} = -8.9° sin(N) + 0.7° sin(2N)

$$\mu_{o1} = 10.8° \sin(N) - 1.3° \sin(2N) + 0.2° \sin(3N)$$

$$\mu_{p1} = 0.0°$$

$$\mu_{q1} = 10.8° \sin(N) - 1.3° \sin(2N) + 0.2° \sin(3N)$$

$$N = (259.16° - 19.3282° (year-1900) - 0.0530° (day + leapyear))$$

Since the calculation of the amplitude and phase of a tidal constituent is relatively time consuming, an interpolation method on a gridded set of pre-calculated results is used instead. The load tide varies smoothly, so it can be interpolated in space and time with negligible error. We calculate the tidal loading at a point (x, y) by first determining its value at the four nearest neighbors in the grid, interpolating the tidal values at the grid points for the appropriate time. Then we use bilinear spatial interpolation (e.g. *Press et al*., 1992) to compute the appropriate amplitude and phase of each tidal component at (x, y). Finally, we combine components using Equation 2.

At each gridded point, the amplitudes and phase of the tidal constituents can be calculated beforehand. Our algorithm is based on the pre- calculation of tides on a 1° by 1° grid globally (this can be performed on a HP-735 workstation of the GLAS Science Computing Facility, using the software described above with no attempt at streamlining the procedure or optimizing the software). When the pre-calculated results are stored on disk, a million points along a ground track, or about 5 orbits, can be calculated in 7 minutes through bilinear interpolation.

Figure 1 shows a grid block for the interpolation. The tidal loading L at point (x, y) is calculated by,

$$L(x, y) = (1-c_1)(1-c_2)L(x_1, y_1)+c_1(1-c_2)L(x_2, y_1)+c_1c_2L(x_2, y_2)+(1-c_1)c_2L(x_1, y_2)$$

$$c_1 = (x-x_1)/(x_2-x_1)$$

$$c_2 = (y-y_1)/(y_2-y_1)$$

Since the load tide varies smoothly, it can be interpolated in space and time with negligible error. This justifies our approach of tabulating load tide amplitudes and phases on a 1°×1° geographical grid. Then, to estimate tidal-loading displacements at any given time and any given point within Antarctica we use bilinear interpolation (e.g. *Press et al.*, 1992) to compute the appropriate amplitude and phase at that location, and use Equation 2. As a check, we compare calculated and interpolated values for a 180-day time series sampled at hourly intervals, starting January 1, 2001, at three locations: (66.6617°S, 140.0014°E), (70.5°S, 135.5°E), and (70.5°S, 45.5°E). The first point is near the coast, the other two are inland. The standard deviations of the residuals between calculated and interpolated values are 0.35 mm, 0.05 mm, and 0.03 mm, respectively. These are well within the accuracy requirements for correcting the measurements to be made by GLAS. In view of these results, it is clear that calculation of the tides at grid nodes

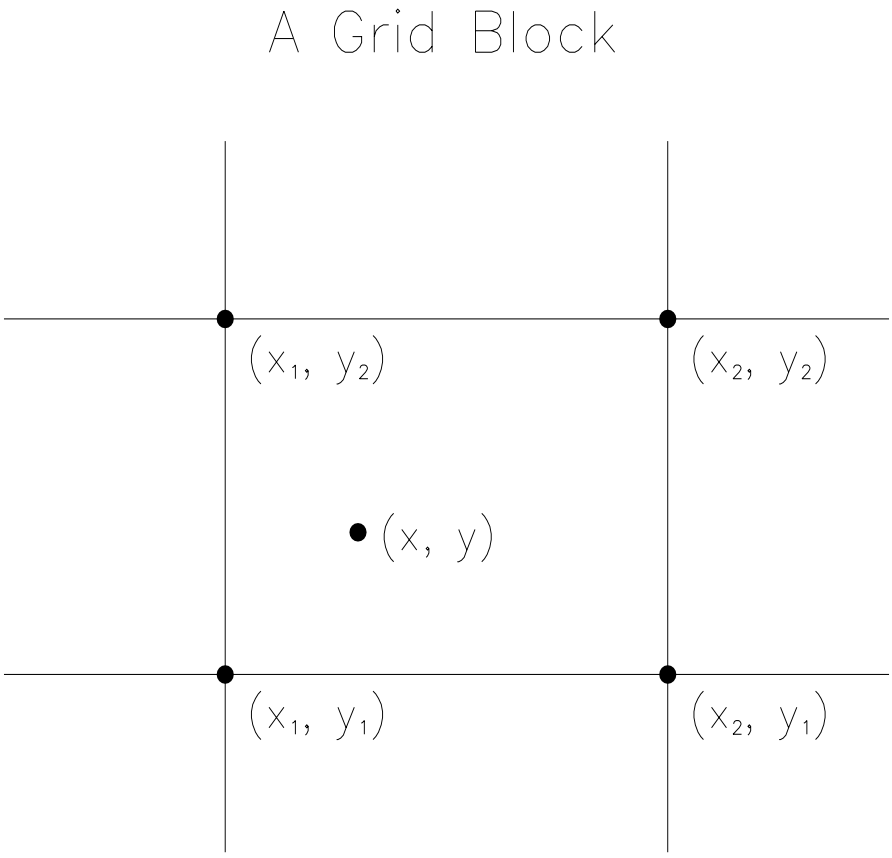

Figure 1: Geometry and notation for bilinear interpolation of ocean load tides.

need only be performed once during the time taken by the spacecraft to traverse the grid cell. This indicates that an effective strategy is to compute the corrections only at a relatively sparse set of points —say, every 15 seconds, that is every 600 shots, or every degree along track— and to interpolate using the shot count as the independent variable along track. This approach will work for any tidal correction, the only caveat being that the transitions from ocean to land environments and *vice versa* must be accounted for by keeping track of the intersections of the ground track with a sufficiently accurate map of the coastlines.

5.5. Discussion

In Equation 2 we accounted for the eight major tidal constituents (four semidiurnal waves: M_2, N_2, S_2, K_2; and four diurnal waves: K_1, O_1, P_1, Q_1) that have the largest contribution to tidal loading. We used the FES95.2 tide model to calculate the amplitude and phase of M_2, N_2, S_2, K_2, K_1, O_1, Q_1. TPXO.2 was used to calculate the amplitude and phase of P_1. We selected FES95.2 mainly because it is a readily available global ocean-tide model which includes the regions under the Ross, Filchner and Ronne Ice Shelves around Antarctica, regions which are of major concern

to the GLAS project.

As a validation of this approach, we compare the vertical displacement computed here to that obtained using amplitude and phase calculated by *McCarthy* (1992) following *Scherneck* (1991). At a test point (66.6617°S, 140.0014°E) in Antarctica, for a 180-day period starting from January 1, 2001, the difference between the two calculations is less than ±1.6 mm. McCarthy's results are estimated to be accurate at the ±3 mm level (*McCarthy*, 1992). Since we used a more recent, presumably improved tide model, we can assume that the accuracy of our calculation is at least as good.

The results show that the vertical tidal loading displacements are typically several centimeters over Antarctica. As expected, the amplitudes are higher along the coast and lower inland. The distribution of the *maximum* possible load tide over Antarctica (the sum of vertical displacements amplitude of eight tide constituents, which is what might be expected if all constituents ever happened to be in phase) is shown in Figure 2. It reaches a maximum value over Antarctica which exceeds 40 mm.

In practice, one sees the largest amplitudes when most of the constituents are in phase. For example at (66°S,100°E) the maximum amplitude is about 40 mm, but the total range of the displacement time series reaches only about 60 mm in the first ten years of the 21st century, not 80

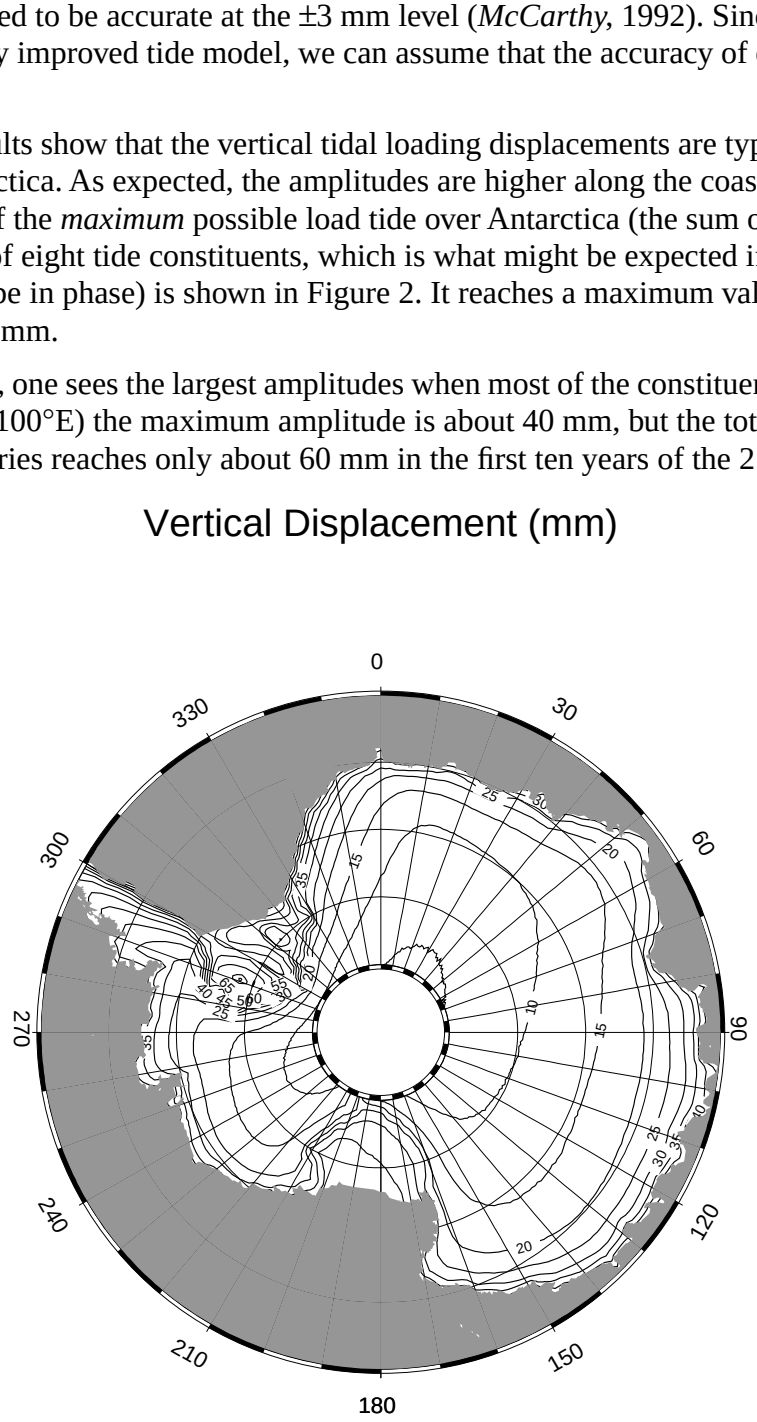

Figure 2: Contour map of maximum vertical displacement due to ocean tidal loading over Antarctica.

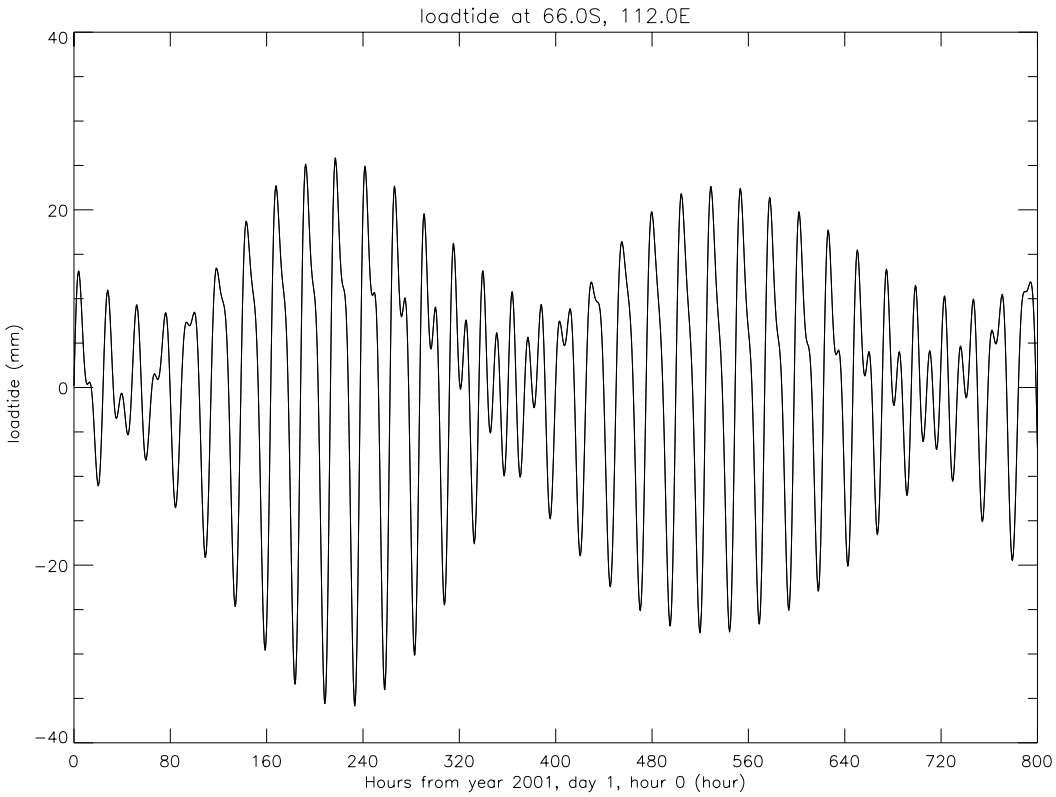

Figure 3: Comparison of load tide time series calculated at 1 hour intervals and at 12 minute intervals. This shows that temporal interpolation is justified.

mm. Figure 3 and Figure 4 are two examples showing the spatial and temporal variations of tidal loading. In Figure 3, two load tide time series are plotted. One is calculated at 1 hour intervals and the other at 0.2 hour intervals. They are indistinguishable, which demonstrates that temporal interpolation is fully justified.

Similarly, in Figure 4, there are two lines plotted: tidal loads calculated every degree and every half degree of longitude, respectively, at latitude 70°S. Again, the two cannot be distinguished. For a time series of 180 days starting from January 1, 2001, at one hour intervals, the standard deviation of the differences between the directly calculated value and the bilinear interpolated value are 0.35 mm, 0.05 mm and 0.03 mm for points at (66.6617°S, 140.0014°E), (70.5°S, 135.5°E), and (70.5°S, 45.5°E). This is good enough for GLAS tidal loading correction.

5.6. Tests of the significance of the loading correction

A standard technique used in altimetry research is crossover analysis. This is done by comparing elevation estimates at successive passes (e.g. ascending and descending measurements) at a single location at the surface. We used a set of crossover points at high southern latitudes, provided by Dr. Schutz's group at University of Texas for an eight day repeat orbit scenario.

Figure 5 shows the tide loading effect over a crossover point at (67.7799°S, 123.1133°E)

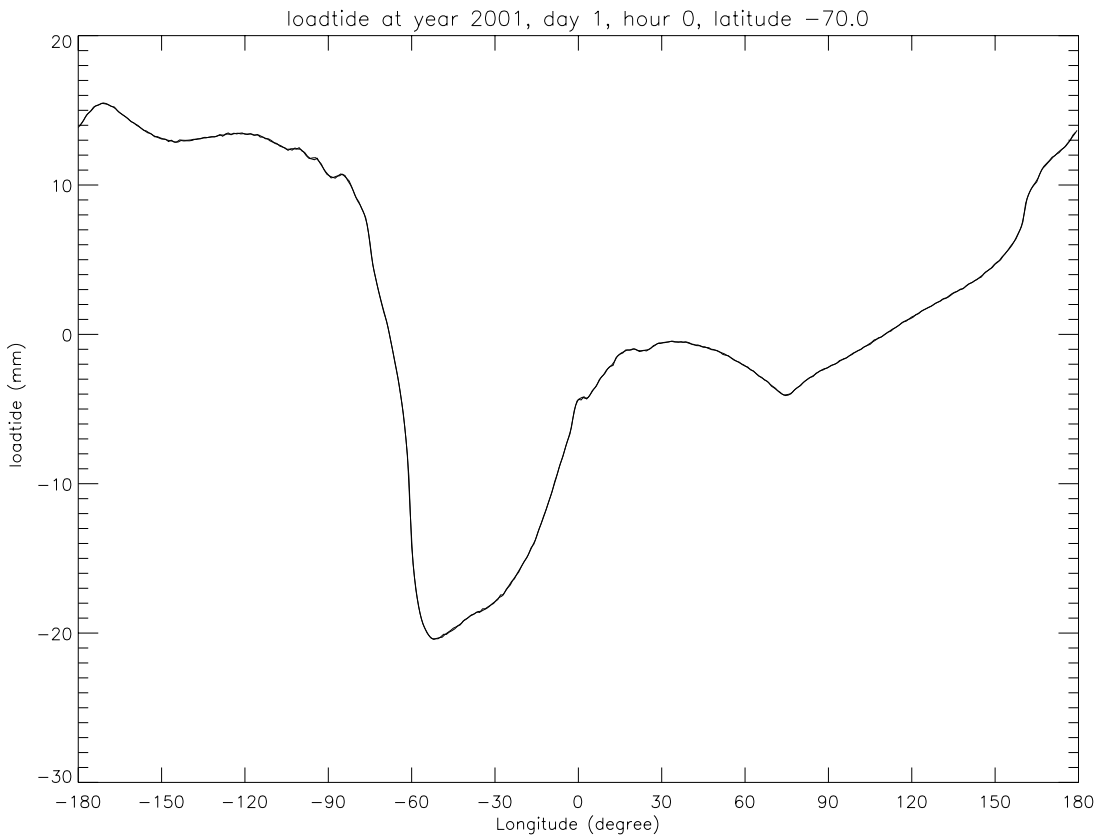

Figure 4. Vertical displacements at epoch 2001 00:00:00, along a small circle of latitude 70°S. Two estimates are shown, calculated at points separated by 1° and 0.5° longitude inter vals, respectively. The excellent agreement justifies the practice of computing load tides on a coarse grid and interpolating bilinearly in space.

for the year 2001. Here we only consider the effect of tidal loading, in order to ascertain whether a beat pattern between tide frequencies and orbital periods might lead to aliased signals masquerading as systematic changes in elevation. Figure 5(a) shows the tidal load variation for the year 2001, starting on January 1, and calculated at one hour intervals. The apparent surface elevation changes for ascending and descending paths at the fiducial point are shown in Figures 5(c) and 5(e). Although individual differences could reach 30 mm, the differences for both ascending and descending passes have means of about zero and standard deviations of about 8 mm (Figures 5d and 5f). This means that if a sufficient number of measurements are used in calculating the surface elevation at this location, for this mission scenario, the bias would be small (several mm). The rms error for a single measurement is found to be less than ±10 mm. The error would be much smaller inland than along the coast.

It is difficult to assess the possibility of biases based on this single calculation. Indeed, there could be instances where the bias could be much more severe. By applying the tidal loading correction discussed above, such possible biases introduced by ocean tidal loading can be avoided. As shown above, ocean tide loading corrections are easily provided along the satellite

ground tracks. Applying these corrections will improve the accuracy of satellite altimeter measured surface elevations over polar regions, especially in the near coast area where the amplitude of the loadtide is larger than inland.

The histogram of these displacement values, shown in frame 5(b) shows that the distribution is significantly skewed at that location, although the mean over the 365-day cycle is very close to zero. This skewness is caused primarily by the near commensurability of the frequencies of certain tide components. (For instance, the histogram of values of the function $\cos\varpi t + \cos 2\varpi t$ is skewed, extending from a minimum of -1.2 to a maximum value of +2.) Furthermore, because this commensurability is nearly perfect for components k1 and k2, this phenomenon may persist with a beat period of many years. It should be noted that the degree of skewness is a function of time, and since it depends on the relative phases of the components, it depends also on location. If the beat period is in turn comparable to the repeat period of the sampling by GLAS, then it is possible for tidal loading signals to appear as small, but geographically coherent long term apparent changes in the average distribution of ice across the ice sheet. It is therefore important to perform this correction accurately. Table 2 shows the frequencies and amplitudes of the tides summed here at our test point, and Table 3 shows the beat periods of the most likely combinations of tides. The actual skewness and its actual geographical distribution is of course a result of the complex pattern of relative phases of all these components.

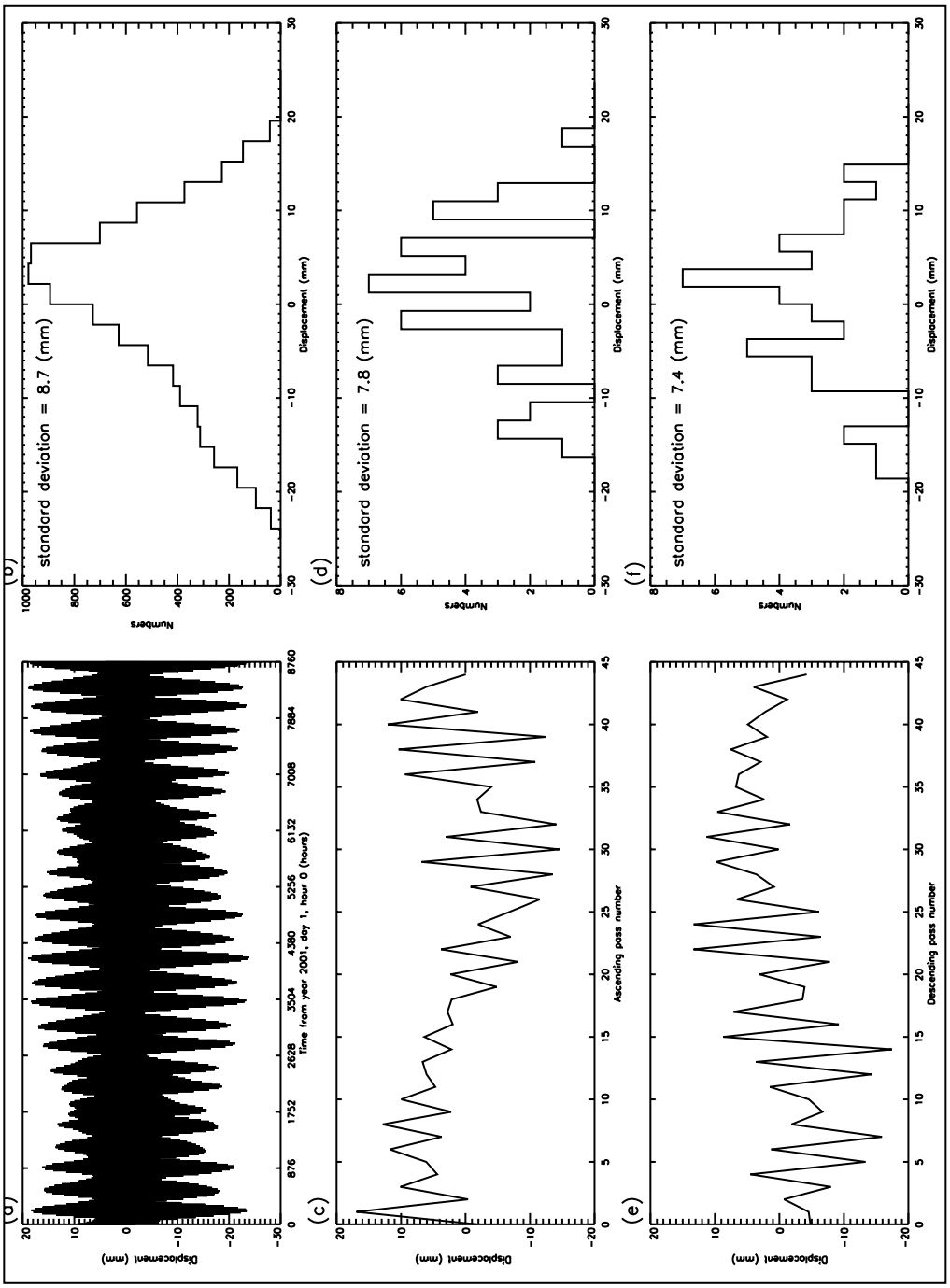

Figure 5: Tidal-loading variations in height and crossover analysis at 67°S, 102°E: (a) tidal-loading height variations for the year 2001; (b) surface-elevation changes at times of ascending-track passage; (c) surface-elevation changes at times of descending-track passage; (d), (e), and (f) histograms for the variations

Table 1: Approximate magnitudes of the components of the tide correction, and their uncertainties

Component	Magnitude	Uncertainty
Ocean tide (open ocean)	±50 cm	±10 cm
Ocean tide (coasts)	±2 m	±10 cm
Ocean tide (ice shelves)	±1 m*	± 40cm*
Long period ocean tide	±1 m (with long period)	few cm
Pole tide	< 2cm	few mm
Ocean-loading tide	±10 cm	< 0.5 cm
Solid Earth tide	±30 cm	±0.5 cm

Values from *Cudlip et al.* (1994).*For Amery Ice Shelf (*Phillips et al* (1999).

.

Table 2: Tide frequencies and vertical displacement at location (67.7799°S, 101.9368°E)

Tide	Frequency (Degree/hour)	Vertical Displacement (mm)
m2	28.9841	4.7
n2	28.4397	1.4
s2	30.0000	2.0
k2	30.0821	0.8
k1	15.0411	7.9
o1	13.9430	7.2
p1	14.9589	2.4
q1	13.3987	1.4

Table 3: Beat frequencies of selected pairs of tidal components

Tide Pairs	Repeat Period (years)
K1 ~ K2	infinity
K2 ~ S2	0.50
P1 ~ S2	0.50
P1 ~ K2	0.25

References

Agnew, D. C., SPOTL: Some programs for ocean-tide loading, *SIO Ref. Ser. 96-8*, 35 pp., Scripps Inst. of Oceanogr., La Jolla, Calif., 1996

Baker, T. F., Method of tidal loading computation, MAREES TERRESTRES. BULLETIN D'INFORMATIONS, **94**, 6365-6373, 1985.

Bentley, C. R. and D. D. Sheehan. Comparison of altimetry profiles over East Antarctic from Seasat and Geosat, an interim report. *Z. Gletscherkd, Glazialgeol.*, **26**(1), 1-9, 1992.

Brenner, A. C., R. A. Bindschadler, R. H. Thomas, and H. J. Zwally, Slope-induced errors in radar altimetry over continental ice sheets. *J. of Geophys. Res*., **88**(c3), 1,617-1,623, 1983.

Cartwright, D.E. and Taylor,R.J., New computations of the tide-generating potential, *Geophys. J. R.Astr.S.oc*., **23**, 45, 1971.

Cudlip, W., D.R. Mantripp, C.L. Wrench, H.D. Griffiths, D.V. Sheehan, M. Lester, R.P. Leigh and T.R. Robinson. Correction for altimeter low-level processing at the Earth Observation data Centre (EODC). *International Journal of Remote Sensing*, **15**, No. 4, pp 889-914.

Doodson, A. T., The analysis of tidal observations. *Phil. Trans. Roy. Soc. Lond.*, **227**, 223-279, 1928

Eanes, R. J., Diurnal and semidiurnal tides from TOPEX/POSEIDON altimetry, *Eos Trans. AGU*, 1994 Spring Meeting Suppl., 108, 1994.

Egbert, G. D., A. F. Bennett, and M. G. G. Foreman, TOPEX/POSEIDON tides estimated using a global inverse model, *J. Geophys. Res.*, **99**, 24821-24852, 1994.

Farrell, W. E., Deformation of the Earth by surface loads, *Rev. Geophysics and Space Phys*., **10**, 761-797, 1972.

Haines, B. J., G. H. Born, R. C. Williamson, and C. J. Koblinsky. Application of the GEM-T2 gravity field to altimetric satellite orbit computation. *J. Geophys. Res.* **99**(c8), 16,237-16,254, 1994.

Jacobs, S. S., Is the Antarctic ice sheet growing? *Nature*, 36029-33, 1992.

Le Provost, C., M. L. Genco, F. Lyard, P. Vincent, and P. Canceil, Spectroscopy of the world ocean tides from a finite element hydrodynamic model, *J. Geophys. Res*., **99**, 24777-24797, 1994.

Le Provost, C., A. F. Bennett, and D. E. Cartwirght, Ocean tides for and fromTOPEX/POSEIDON, *Science*, **267**, 639-642, 1995.

Le Provost, C., F. Lyard, J. M. Molines, M.L. Genco and F. Rabilloud. A hydrodynamic ocean tide model improved by assimilating a satellite-altimeter-derived data set, *J. Geophys. Res.*, **103**, 5513-5529, 1998.

Lingle, C. S., L. Lee, H. J. Zwally, and T. C. Seiss. Recent elevation increase on Lambert Glacier, Antarctic, from orbit crossover analysis of satellite radar altimetry. *Ann. Glacial*., **20**, 26-32, 1994.

McCarthy, D. D. (ed), IERS Technical Note 13, 1992.

Oerlemans, J. Possible changes in the mass balance of the Greenland and Antarctic ice sheets and their observations, projections and implications. Edited by R. A. Warrick, E. M. Barrow and T.M. L. Wigley. Cambridge University Press. 424 pp. 1993.

Partington, K. C., W. Cudlip, and C. G. Rapley. An assessment of the capability of the satellite radar altimeter for measuring ice sheet topographic change. *Int. J. Remote Sensing*, **12**(3), 585-609. 1991.

Phillips, H.A, I. Allison, R. Coleman, G. Hyland, P.J. Morgan and N.W. Young. Comparison of ERS satellite radar altimeter heights with GPS-derived heights on the Amery Ice Shelf, East Antarctica. *Annals of Glaciology*, **27**, 19-24, 1998.

Phillips, H.A, G. Hyland, R. Coleman and N.W. Young. Digital Elevation Models for the Lambert Glacier-Amery Ice Shelf system, East Antarctica, from ERS-1 satellite radar altimetry. Submitted to *Journal of Glaciology*, August 1999.

Press, W. H., S. A. Teukolsky, W. T. Vetterling, and B. P. Flannery, Numerical Recipes in C. Cambridge University Press, New York, 994 pp., 1992.

Ridley, J. K. and K. C. Partington. A model of satellite radar altimeter return from ice sheets. *Int. J. Remote Sensing.* **9**(4), 601-624, 1988.

Rignot, E. Radar interferometry detection of hinge-line migration on Rutford Ice Stream and Carlson Inlet, Antarctica. *Annals of Glaciology*, **27**, 25-32, 1998.

Rignot, E., L. Padman, D.R. MacAyeal and M. Schmeltz. Analysis of sub-ice-shelf tides in the Weddell Sea using SAR imterferometry. Submitted to *J. Geophys. Res.*, 1999.

Robertson, R., L. Padman and G. Egbert. Tides in the Weddell Sea. In *Ocean, Ice, and Atmosphere: Interactions at the Antarctic Continental Margin*, Antarctic Research Series, **75**, pp. 341-369, 1998.

Scherneck, H. G., A parameterized solid earth tide model and ocean tide loading effects for global geodetic baseline measurements, *Geophys. J. Int.*, **106**, 677-694, 1991.

Schutz, B. E. Geoscience Laser Altimeter System. MTPE/EOS Reference Handbook. 123-134, 1995.

Schwiderski, E. W., On charting global ocean tides, *Rev. of Geophys. and Space Phys.*,**18**. No. 1, 243-268, 1988.

Shum, C.K., P.L. Woodworth, O.B. Anderson, G.D. Egbert, O. Francis, C. King, S.M. Klosko, C. Le Provost, X. Li, J-M Molines, M.E. Parke, R.D. Ray, M.G. Schlax, D. Stammer, C.C. Tierney, P. Vincent and C.I. Wunsch, Accuracy assessment of recent ocean tide models, *J. Geophys. Res.*, **102**, 25173-25194, 1997.

Vaughan, D.G., Investigating tidal flexure on an ice shelf using kinematic GPS. *Annals of Glaciology*, **20**, 372-376, 1994.

Vaughan, D.G., Tidal flexure at ice shelf margins. *J. Geophys. Res.*, **100**(B4), 6213-6224, 1995

Warrick, R. A., Climate and sea level change: a synthesis. Climate and sea level change: Observations, projections, and implications. Edited by R. A. Warrick, E. M. Barrow and T. M. L. Wigley. Cambridge University Press. 424 pp. 1993.

Warrick R. A. and J. Oerlemans. Sea level rise. Climate change, the ICPP Scientific Assessment. Edited by J. T. Houghton, G. T. Jenkins and J. J. Ephraums. Cambridge University Press. 365, pp. 1990.

Wessel, P., and W. H.F. Smith. A global, self-consistent, hierarchical, high-resolution shoreline database, *J. Geophys. Res.*, **101**, 8741 - 8743, 1996.

Yi, D. and C. R. Bentley. A retracking algorithm for satellite radar altimetry over an ice sheet and its applications. *Glaciers, Ice Sheets, and Volcanoes: A Tribute to Mark F. Meier.* Edited by S. C. Colbeck. U.S. Army Cold Regions Research and Engineering Laboratory, Special report 96, **27,** 112-120, 1997.

Yi, D., C. R. Bentley, and M. D. Stenoien. Seasonal variation in the height of the East Antarctic ice sheet. *Ann. Glaciol.*, ***24,*** *191-198*, 1997.

Zwally, H. J., Growth of Greenland ice sheet: interpretation. *Science*, **246**(4937), 1,589-1,591, 1989.

Zwally, H. J., A. C. Brenner, J. A. Major, R. A. Bindschadler, and J. G. Marsh. Growth of Greenland ice sheet: Measurement. *Science*, **246**(4937), 1,587-1,589, 1989.

Zwally, H. J., A. C. Brenner, J. A. Major, T. V. Martin and R. A. Bindschadler. Satellite radar altimetry over ice. Vol. 1, Processing and corrections of Seasat data over Greenland, Washington, DC, National Aeronautics and Space Administration. (NASA Ref. Pub. 1233, 1.)